EUROPEAN FUSION DEVELOPMENT AGREEMENT

EFDA–JET–CP(03)01-17

W. Fundamenski, S. Sipilä
and JET EFDA Contributors

Classical versus Anomalous SOL Transport in JET ELMy H-Modes

Classical versus Anomalous SOL Transport in JET ELMy H-Modes

W. Fundamenski, S. Sipilä
and JET EFDA Contributors*

Euratom/UKAEA Fusion Association, Culham Science Centre, Abingdon, Oxon, UK
1Helsinki U. of Technology, Tekes-Euratom Assoc., PO Box 2200, FIN-02015 HUT, Finland
**See Annex of J. Pamela et al., "Overview of Recent JET Results and Future Perspectives", Fusion Energy 2000 (Proc. 18th Int. Conf. Sorrento, 2000), IAEA, Vienna (2001).*

Preprint of Paper to be submitted for publication in Proceedings of the
EPS Conference on Controlled Fusion and Plasma Physics,
(St. Petersburg, Russia, 7-11 July 2003)

INTRODUCTION.

The radial extent of a magnetised boundary plasma, or scrape-off layer (SOL), is determined by competition between transport processes parallel ($\|$) and perpendicular (λ) to the magnetic field B [1]. Whereas most aspects of $\|$ transport are well understood, $\perp$ transport is generally anomalous, determined largely by turbulent processes [1]. In nuclear fusion devices, the radial extent of the SOL determines the peak heat flux on the divertor tiles which poses a key constraint on the design and successful operation of next-step tokamaks, such as ITER [2]. In order to improve our predictive capability, physical understanding of the underlying $\perp$ transport mechanisms is essential, especially in the reference regime of ITER, the so called ELMy H-mode [3]. With this aim, a series of experiments were carried out on JET in which power deposition widths λ_q were measured in several D and He plasmas, including scans in toroidal B_ϕ and poloidal B_θ fields, the latter expressed as a magnetic safety factor $q_{95} \sim aB_\phi/RB_\theta$, neutral beam power P_{NB} and line average density $<n_e>$.

1. EXPERIMENTAL RESULTS.

Power widths λ_q were measured for 22 discharges in total (16D, 6He), consisting of 19 H-modes and 3 L-modes. All plasmas had identical shape and the direction of toroidal field with $\mathbf{B}\times\nabla\mathbf{B}$ towards the divertor. The heating power varied by a factor of four, while the line-average density changed by a factor of two, spanning the Greenwald fraction f_{GW} from ~0.3 in L-mode, through ~0.6 in D H-modes, up to the ITER relevant values of 0.8-1.0 in He H-modes.

ELM-averaged power deposition profiles were obtained for each of the above discharges using the swept strike-point thermocouple (TC) technique [5,6], which agrees closely with the infra-red (IR) diagnostic [7]. Since ELMs are responsible for only ~20-30% of the energy reaching the divertor targets [8], these profiles are dominated by inter-ELM energy transport. In addition, electron power profiles were measured using the divertor Langmuir probes (LP), $q_e = 5T_e\Gamma_0$ [6,9]. The profiles are parametrized in terms of two variables: peak heat flux q_0 and the integral width, defined as $\lambda_q \equiv \int q dr / q_0$. Upstream quantities of $T_{e,u}$, $T_{i,u}$ and $n_{e,u}$ have been calculated using two-point model estimates [11,12] based on target LP measurements of Te,t and ne,t, and total target power from TC. It was found that in D H-modes ions were only marginally collisional ($\nu^*_i < 3$), whereas in He plasmas $\nu^*_i > 30$. The electrons were collisional throughout, $\nu^*_e > 30$.

2. STATISTICAL ANALYSIS.

Standard regression analysis was performed on TC and LP widths with respect to ion mass A and charge Z, B_ϕ, q_{95}, P_t and $n_{e,u}$. Since A/Z=2 for both D^+ and He^{++}, one of these variables is redundant in the regression; we shall denote this by writing A(Z). The choice of Pt and ne,u as the two plasma variables was dictated by three factors: a) continuity with literature [3], b) accuracy of estimates, c) comparison with theory. The following scaling was obtained,

$$\lambda_q^{TC} \propto A(Z)^{1.04}\, B_\phi^{-1.03}\, q_{95}^{0.60}\, P_t^{-0.41}\, n_{e,u}^{0.25}.$$

Little difference in the regression was found by excluding the L-mode points. The LP width showed similar scaling with A(Z) with weaker dependance on other variables, so that λ_q LP $\propto A(Z)B_\theta^{-0.3}$. In what follows, we restrict our analysis to λ_q^{TC} alone.

3. SIMPLE MODEL OF THE SOL (UNIFORM GRADIENTS).

Local power balance in the SOL in the absence of sources may be written as $\nabla_\| q_{\|\alpha} + \nabla_\perp q_{\perp\alpha} = 0$, where $q_{\|\alpha} = {}^1/_2(m_\alpha v_\alpha^2 + 5T_\alpha)n_\alpha v_{\|\alpha} - n_\alpha \chi_{\|\alpha} \nabla_\| T_\alpha$ and $q_{\perp\alpha} = - n_\alpha \chi_{\perp\alpha} \nabla_\perp T_\alpha$ are the $\|$ and $\perp$ energy fluxes for species $\alpha \in \{e,i\}$, $\chi_{\|\alpha} \propto T_\alpha \tau_\alpha / m_\alpha$ and $\chi_{\perp\alpha}$ are the $\|$ and $\perp$ heat diffusivities [1]. The above may be simplified by replacing the $\|$ and $\perp$ gradients by inverse lengths $1/L_\|$ and $1/\lambda_{q\alpha}$, where $\lambda_{q\alpha}$ is the power e-folding length in the SOL. This yields an expression for $\lambda_{q\alpha} \sim (n_\alpha T_\alpha L_\| \chi_{\perp\alpha} / q_{\|\alpha})^{1/2}$. Introducing the convective and conductive times ($\tau_{v\alpha} \sim L_\| / v_{\|\alpha}$, $\tau_{\chi\alpha} \sim L_\|^2 / \chi_{\|\alpha}$), one can express the condition for $\|$ heat transport being dominated by convection as $\Xi \equiv \tau_v / \tau_\chi < 5/2$. We approximate the former as $\tau_v \sim L_\| / Mc_s$ where $c_s = \{(ZT_e + T_i)/m_i\}^{1/2}$ is the plasma sound speed and $M = v_\| / c_s$ is the Mach number; over the range $1<Z<2$, cs scales as $\{Z^\xi / A\}^{1/2}$ with $\xi=0.6$ for $\vartheta=1$ and $\xi=0.42$ for $\vartheta=2$. The latter becomes $\tau_\chi \sim L_\|^2 / \chi_{\|e}$ since $\chi_{\|e} / \chi_{\|i} \sim 35 A^{0.5} Z^3 \vartheta^{-2.5}$, which gives ~ 10 for D^+ and ~ 100 for He^{++} (M~0.5 and ϑ~2 will be assumed henceforth in light of evidence for strong SOL flows and energetic ions in the SOL [7,13]). In the convective regime ($\Xi < 5/2$), the power width becomes $\lambda_{qv,\alpha} \sim (\chi_{\perp\alpha} L_\| / c_s)^{1/2}$; in the conductive regime ($\Xi > 5/2$), one obtains $\lambda_{q\chi,\alpha} \sim L_\| (\chi_{\perp\alpha} / \chi_{\|e})^{1/2} (T_\alpha / T_e)^{1/2}$. On the basis of Ξ evaluated at both the upstream and target locations for all discharges ($\Xi_u \sim 10$, $\Xi_t \sim$ 1), we expect conduction to dominate in the upstream SOL ($q_\| \sim nc_\| e\tilde{N}_\| Te$) and convection in the divertor region ($q_{\|\alpha} \sim 2.5 T_\alpha n_\alpha Mc_s$). Both expressions for λ_q are thus relevant for the present study.

4. NUMERICAL MODEL OF THE SOL (EDGE2D).

The above simple expressions were compared with results of a 2-D numerical transport code, solving the fluid-like Braginskii equantions in the SOL, on an EFIT matching mesh. Over 50 simulations were performed, involving scans in A={1-3}; P_i, P_e = {2-6} MW; $n_{e,u}$ = {1-4}$\times 10^{19}$ m^{-3}; $D_\perp = \chi_{\perp,e} = \chi_{\perp,i}$ = {0.1-1.0} m^2/s. The obtained width λ_q^{EDGE2D} ~ was best matched with the $\|$ conduction expression evaluated with upstream quantities, $\lambda_{q,\chi}^{u}$, Fig.1. Comparable match was found with $\|$ convective width evaluated with target quantitieslq,vt, in agreement with expectations. We may conclude that the simple model offers a fair approximation to the power width. An additional insight into, $\|$ transport in the SOL may be gained by noting that $\tau_\| \sim \lambda_q^2 / \chi_\perp$ correlates strongly with upstream collisionality, t$\|$ ~ $\nu^{*1.5}_{i,u} \sim \nu^{*2.2}_{e,u}$, Fig.2. This suggests that $\|$ transport in the main SOL is governed by $\|$ conduction

5. MODELS OF $\perp$ ENERGY TRANSPORT.

Following the approach of Connor et al. [14,15], two dozenmodels for $\perp$ heat diffusivity $\chi_\perp$ were considered. The model notation of [14] was retained, withthree notable additions: the classical **A1** and neo-classical **A2** ion conduction, as well as classical electron conduction **A3**. For a detailed description of the underlying physics of each model, the reader should consult [14] and the citations

contained therein. Also included in Table 3, are scalings of ion toroidal ri (**Y1**) and poloidal rqi (**Y2**) gyro-radii, and electron toroidal re (**Z1**) and poloidal rqe (**Z2**) gyro-radii. Finally, the footprint of IOL on the outer target was obtained via numerical simulations of JET plasmas using the ASCOT code [16]. Over thirty simulations were performed with $1.5T < B_\phi < 3.5T$, $2.6 < q_{95} < 5.2$, $A \leq 12$ and $Z \leq 2$, to yield the following expression:

$$\lambda_q^{IOL}\,[\text{mm-omp}] = 2.2A^{0.35\pm0.03}\, Z^{-0.8\pm0.06}\, B_\phi^{-0.89\pm0.04}\, q_{95}^{0.88\pm0.04}\, T_i^{0.39\pm0.1}\, n_e^{-0.08\pm0.1}$$

Not surprisingly, the resulting width, denoted by **X**, scales roughly as the poloidal gyro-radius $\rho_{\theta i}$ (**Y2**), i.e. as the banana width, the differences arising mainly from topological effects associated with the X-point. The above models can be categorized into four families of increasing order of complexity: a) **Q**, $\lambda_\perp$ =constant; b) **X-Z**, λ_q~ gyro-radii; c) A, (neo-)classical conduction, d) **B-O**, anomalous.

6. COMPARISON WITH EXPERIMENT.

The above $\chi_\perp$ models were introduce into the $\lambda_{q,v}$ and $\lambda_{q,\chi}$ expressions derived previously. For a general scaling $\chi_\perp \propto A^{\mu} Z^{\eta} B^{\xi} L_\parallel^{\zeta} n_e^{\psi} T_\alpha^{\theta} \lambda_{q,s}$, one obtains the results $\lambda_q \propto (A^x Z^y B^z L_\parallel^{w} n_{eu} T_\alpha^{v})^s$ where $x = (\mu + 0.5)/2$, $y = (\eta - 0.21)/2$, $w = (\zeta + 1)/2$, $u = (\psi+1)/2$, $v=(q-2.5)/2$ for $\lambda_{q,\chi}$; $x = \xi/2$, $y = h/2$, $w = 1+z/2$, $u = y/2$, $v = (q-0.5)/2$ for $\lambda_{q,c}$, and $z = x/2$, $s = 1/(1+\sigma/2)$ for both. In what follows, we introduce the following notation: $\perp$ model **A** with $\parallel$ assumption a will be termed a mechanism and denoted as **A:a**. As a figure of merit of the comparison we take the RMS difference Δ between the predicted (model) and measured (regression) exponents. This quantity Δ is plotted in ascending order for the best ten models assuming $\parallel$ convection, $\lambda_{q,v}$, Fig.3, and $\parallel$ conduction, $\lambda_{q,c}$, Fig.4. The best match to the experiment is offered by classical ion conduction **A1** ($\Delta_{A1:v} = 0.10$, $\Delta_{A1:\chi} = 0.29$), which alone shows shows significant improvement over the null model Q. It is followed by resistive MHD (interchange E and drift ballooning turbulence **H**), classical electron conduction **A3**, Bohm **N**, $\rho_{\theta e}$ **Z2**, endplate MHD (**B2, G2**), skin depth **I** and others. The breakdown of Δ into primary components, reveals that over models **B** to **Z**, DA(Z) is by far the largest source of discrepancy.

DISCUSSION.

The above results point to two leading **A1:**{**v,χ**} and several secondary, Σ {**E,H,A3,N,B2,…**}:{**v,χ**}, energy transport mechanisms in the SOL plasmas considered. Radial transport appears to be dominated by classical ion conduction, with electron conduction playing a supplementary role. The latter contains both classical and turbulent-electrostatic (resistive, ballooning, interchange) contributions. Net energy flow from the ion into the electron channels is implied, eg. **A1(i)**: **χ(e)**. On the particle scale, **A1** involves diffusion of energy with radial steps of the ion gyro-radius occurring with i-i collision frequency, $\chi_\perp^{i} \sim \rho_i^2\, \nu_{ii}$, which implies a quiescent plasma (consistent with the observed reduction in fluctuations of density and potential in the vicinity of the separatrix

in H-modes [17]) of sufficient collisionality to assure several diffusive steps. The average number of diffusive steps $N_{\perp,\alpha}$ for species $\alpha \in \{e,i\}$ is just the ratio of $\|$ and collisional times, $N_{\perp,\alpha} \sim \tau_{\|\alpha} / \tau_{\alpha\alpha}$, so that $N_{\perp,e} \sim L_{\|}^{2}/\chi_{\|}^{2}\tau_e \sim \nu^{*}_{e}{}^{2}$ while $N_{\perp,i} \sim L_{\|}/c_s\tau_i \sim \nu^{*}_{i}$. Consequently, the diffusive approximation is valid for most discharges ($\nu^{*}_{i} > 3$). Since $103 \sim N_{\perp,e} >> N_{\perp,i} \sim 2\text{-}50$, one may speculate that the onset of turbulence occurs above some critical $N_{\perp,\alpha} \sim 30\text{-}10^3$. Both numbers approach unity as $\nu^{*}_{\alpha} \rightarrow 1$ and zero as $\nu^{*}_{\alpha} \rightarrow 0$. In this limit, the power width should reduce to a combination of gyro-radii expressions **X-Z**. In fact, ion orbit loss **X** ~ $\rho_{\theta i}$(**Y2**) has been identified as the cause of deposited power profile peaking (narrow λ_q) in high power D H-modes (eg. 50397), for which $\nu^{*}_{i} < 3$ [7]. Consequently, under quiescent conditions classical ion transport reduces to IOL in the collisionless limit, **A1:v** $\rightarrow$ **X** as $\nu^{*}_{i} \rightarrow 0$. The composite picture can be drawn as follows,

$$(\nu^{*}_{e} > 10, \nu^{*}_{i} > 3) \quad \Rightarrow \quad \textbf{A1:v} \quad > \quad \{A1{:}\chi, \Sigma\}$$
$$(\nu^{*}_{e} > 10, \nu^{*}_{i} < 1) \quad \Rightarrow \quad \textbf{A1:v} \rightarrow \textbf{X} \quad >> \quad \{A1{:}\chi, \Sigma \rightarrow 0, \Sigma\}$$

Note that ion and electron channels become de-coupled as $\nu^{*}_{i} < 1$, since $\nu_{ie} << \nu_{ii}$ [10].

Including the magnitude in the comparison, the measured widths are well matched by $\lambda_q^{TC}/\lambda_q^{A1:v} \sim 2.25 \pm 0.45$, which is not far away from unity. An impoved fit is obtained with a collisionaly modified orbit loss expression, $\lambda_q^{TC}/\lambda_q^{X}\, \nu^{*0.5}_{i} \sim 1.0 \pm 0.2$, supporting the hypothesis that **A1:v** $\rightarrow$ **X** in the collisionless limit. The two mechanisms may be combined into a transitional estimate,

$$\lambda_q^{\textbf{A1-X}} = \xi \times C_{A1:v}\lambda_q^{\textbf{A1:v}} + (1\text{-}\xi)\lambda_q^{\textbf{X}},\ \xi \equiv \nu^{*}_{i} / (1 + \nu^{*}_{i}),\ C_{A1:v} \sim 2.4,$$

which gives an equally good match to JET data, $\lambda_q^{TC}/\lambda_q^{\textbf{A1-X}} \sim 1.0 \pm 0.2$. cf. the ITER design value of 5mm-omp. The above expressions predict $\lambda_q^{ITER} \sim 3 \pm 1$mm-omp. In light of the increased closure (higher plasma/neutral compression) of the ITER divertor, this estimate represents λ_q at the entrance into the divertor volume, and thus a lower limit on the deposited power width.

CONCLUSIONS.

Analysis of recent JET experiments presented in this study provides strong evidence for the reduction (suppression?) of ion turbulence in the vicinity of the separatrix in ELMy H-modes. Radial transport is dominated by classical ion conduction for $\nu^{*}_{i} > 3$, which reduces to ion orbit loss for $\nu^{*}_{i} < 1$. Based on these results, the ITER power width can be estimated as 3-4 mm-omp at the entrance into the divertor volume. The accuracy of this prediction will be improved in a future study, by including the above mechanisms in an existing edge transport code.

REFERENCES

[1]. P.C.Stangeby, The Plasma Boundary of Magnetic Fusion Devices, IoP Publishing (2000).

[2]. R.Aymar, The ITER design, Plasma Phys. Contr. Fusion, **44** (2002) 519.

[3]. ITER database, many authors, Nuclear Fusion, **39** (1999), 2423.

[4]. K.McCormick et al., J. Nucl. Mat., **266** (1999), 99.
[5]. V.Riccardo et al., Plasma Phys. Contr. Fusion, **43** (2001), 881.
[6]. W.Fundamenski, Plasma Phys. Contr. Fusion, **44** (2002), 761.
[7]. W.Fundamenski et al., 15th Plasma-Surface Int. Conf. (Gifu, Japan, 2002).
[8]. G.F.Matthews et al., J. Nucl. Materials, **290-293** (2001), 668.
[9]. R.D.Monk, "Langmuir Probe Measurements in the Divertor Plasma of the JET tokamak", Ph.D. Thesis, Imperial College London (1996).
[10]. K.Miyamoto, Plasma Physics for Nuclear Fusion, MIT Press (1987).
[11]. W.Fundamenski, "Tokamak Edge Plasma Modelling Using an Improved Onion-Skin Method", Ph.D. Thesis, U.Toronto (1999).
[12]. W.Fundamenski, J. Nucl. Materials, **290-293** (2001), 593.
[13]. A.Chankin, , J. Nucl. Materials, **290-293** (2001), 518.
[14]. J.W.Connor et al., Nuclear Fusion, **39** (1999), 169.
[15]. G.Councell, J. Nucl. Materials, **266-269** (1999), 91.
[16]. J.A.Heikkinen, Phys.Plasmas, **8** (2001), 2824.
[17]. J.W.Connor et al., Plasma Phys. Contr. Fusion, **42** (2000), R1.

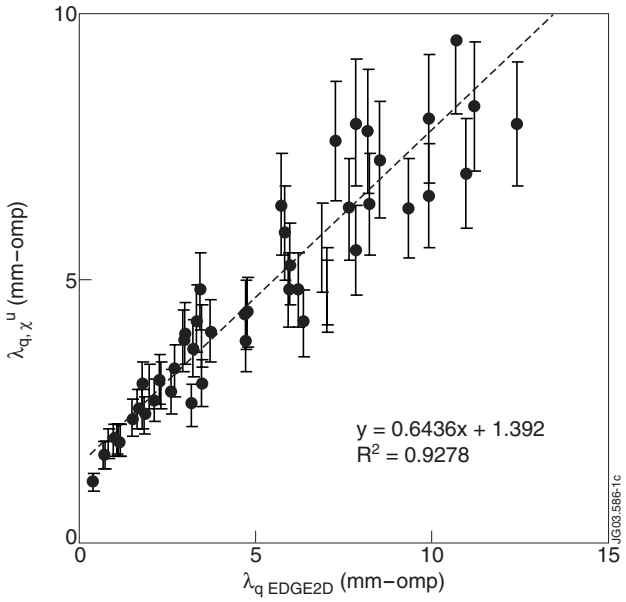

Figure 1: Simple power width expression $\lambda_{q,\chi}{}^{u}$ versus numerical result λ_q^{EDGE2D}.

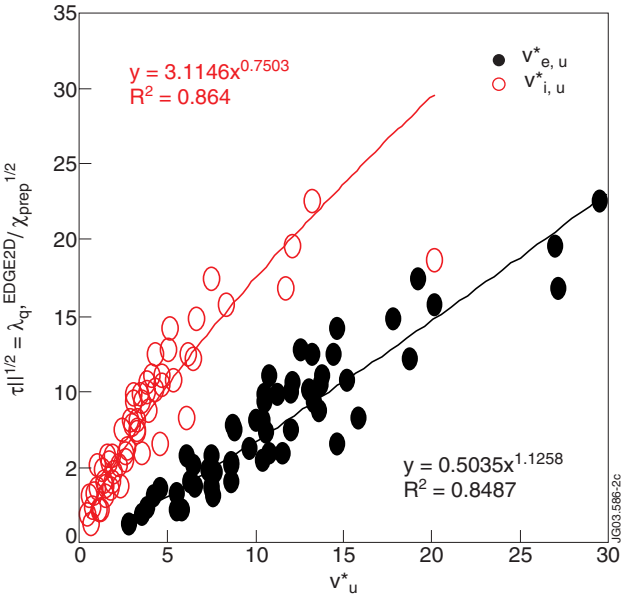

Figure 2: EDGE2D ‖ transport time vs. upstream ion and electron collisionality.

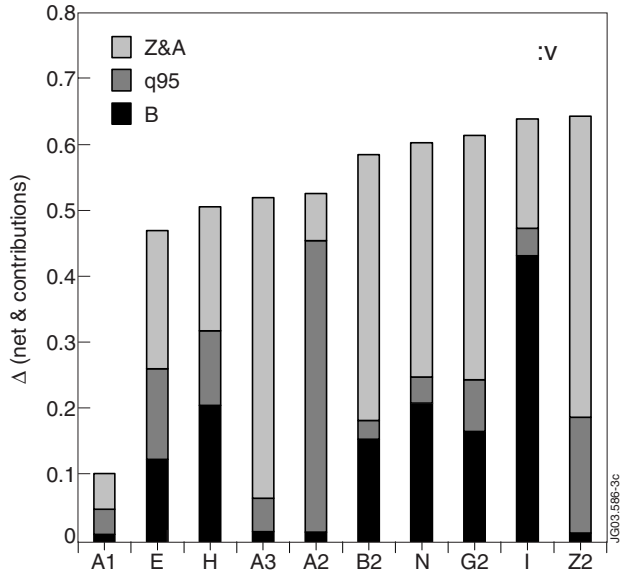

*Figure 3: RMS difference D between the model and regression exponents, assuming || convection (**:v**), along with contributions from Z(A), q_{95} and B_ϕ exponents.*

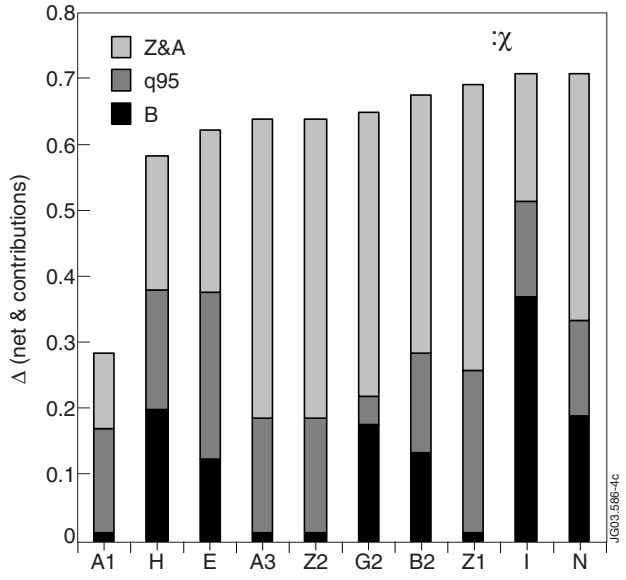

Figure 4:Same as Fig.4 but assuming ‖ conduction (:χ).